

# ANKRD11 binding to cohesin suggests a connection between KBG syndrome and Cornelia de Lange syndrome

Haiyang Liu<sup>a,b</sup>, Hao Li<sup>c,d</sup>, Qixu Cai<sup>e</sup>, Jie Zhang<sup>f</sup>, Hongxin Zhong<sup>f,g,h</sup>, Gongcheng Hu<sup>g</sup>, Shuaizhu Zhao<sup>c,d</sup>, Yuli Lu<sup>f,h</sup>, Yudi Mao<sup>a,b</sup>, Youming Lu<sup>c,d</sup>, Hongjie Yao<sup>g</sup>, and Mingjie Zhang<sup>a,b,1</sup>

Affiliations are included on p. 11.

Edited by Liqun Luo, Stanford University, Stanford, CA; received August 26, 2024; accepted December 23, 2024

Ankyrin Repeat Domain-containing Protein 11 (ANKRD11) is a causative gene for KBG syndrome, a significant risk factor for Cornelia de Lange syndrome (CdLS), and a highly confident autism spectrum disorder gene. Mutations of ANKRD11 lead to developmental abnormalities in multiple organs/tissues including the brain, craniofacial and skeletal bones, and tooth structures with unknown mechanism(s). Here, we find that ANKRD11, via a short peptide fragment in its N-terminal region, binds to the cohesin complex with a high affinity, implicating why ANKRD11 mutation can cause CdLS. The crystal structure of the ANKRD11 peptide in complex with cohesin, together with biochemical experiments, revealed that ANKRD11 competes with CCCTC-binding factor in binding to the cohesin complex. Importantly, a single point mutation in ANKRD11 (Tyr347 to Ala) specifically disrupted the interaction between ANKRD11 and cohesin and perturbed gene expressions in a mouse embryonic stem cell model. Mice carrying the ANKRD11 Y347A mutation display neural and craniofacial anomalies, which mirror clinical phenotypes observed in KBG syndrome patients. Thus, our study reveals how ANKRD11 functions together with cohesin to regulate gene expression and also provides insights into the molecular mechanisms underpinning developmental disorders caused by ANKRD11 mutations.

ANKRD11 | cohesin | KBG syndrome | Cornelia de Lange syndrome

KBG syndrome patients, caused by mutations in the Ankyrin Repeat Domain-containing Protein 11 (ANKRD11) gene, manifest a broad spectrum of clinical features such as craniofacial, skeletal, and dental anomalies, intellectual disabilities, epilepsy, autism, etc. (1-8). ANKRD11 mutations have also been identified in individuals with Cornelia de Lange Syndrome (CdLS), a more severe multisystem developmental disorder characterized by physical development delays, distinct facial features, and intellectual disabilities (9-11). CdLS is caused by mutations in the cohesin complex subunits [such as Nipped-B-like (NIPBL), Structural Maintenance of Chromosomes 1A (SMC1A), Structural Maintenance of Chromosomes 3 (SMC3), RAD21 Cohesin Ring Component (RAD21)] and its regulators (like Histone Deacetylase 8), as well as non-cohesin genes including Bromodomain-containing Protein 4 (BRD4) and ANKRD11 (9, 12–15). The clinical phenotype overlaps of patients with mutations in ANKRD11 and genes encoding the cohesin complex imply a functional or possibly physical interaction between ANKRD11 and cohesin (16).

ANKRD11 encodes a huge nuclear protein characterized by a conserved N-terminal region and a conserved  $\alpha$ -helix-rich C-terminal region, connected by an extended (aa 650 to 2,347), evolutionarily less conserved, and unstructured middle region (Fig. 1A). The N-terminal region contains a bipartite nuclear localization signal essential for nuclear import and four ankyrin repeats with unknown functions (17, 18). The C-terminal helical region is crucial for the protein's stability and recruitment of the Histone Deacetylase 3 complex to the ANKRD11-bound transcription sites. The known disease-causing missense mutations of ANKRD11 are enriched in the C-terminal region directly responsible for gene transcriptions (SI Appendix, Fig. S1) (19, 20). In mice, ANKRD11 plays crucial roles in neuronal development and craniofacial bone formation, correlating well with clinical observations in KBG syndrome patients caused by ANKRD11 mutations (19). Conditional loss of one allele of ANKRD11 in neural crest cells results in pronounced craniofacial developmental anomalies and congenital heart defects in mice (21, 22). Moreover, mice with an N-ethyl-N-nitrosourea-induced heterozygous missense mutation in the C terminus of ANKRD11 exhibit craniofacial defects, including a persistently open anterior fontanelle, highlighting ANKRD11's critical role in craniofacial development (23).

## **Significance**

Neurodevelopmental disorders, including autism, typically exhibit complex phenotypes and genetic backgrounds, making mechanistic studies challenging. This study identifies a direct interaction between Ankyrin Repeat Domain-containing Protein 11 (ANKRD11) and the cohesin complex, elucidating a crucial molecular mechanism underlying developmental disorders such as KBG syndrome and Cornelia de Lange syndrome (CdLS). By demonstrating how a specific mutation in ANKRD11 disrupts this interaction and alters gene expression, our research highlights ANKRD11's essential role in regulating neural and craniofacial development and explains why ANKRD11 mutations can cause KBG syndrome and CdLS.

Author contributions: H. Liu., Youming Lu, H.Y., and M.Z. designed research; H. Liu, H. Li, Q.C., J.Z., H.Z., G.H., S.Z., Yuli Lu, and Y.M. performed research; H. Liu, H. Li, Q.C., J.Z., H.Z., G.H., S.Z., Yuli Lu, Youming Lu, H.Y., and M.Z. analyzed data; and H. Liu and M.Z. wrote the paper.

The authors declare no competing interest.

This article is a PNAS Direct Submission.

Copyright © 2025 the Author(s). Published by PNAS. This article is distributed under Creative Commons Attribution-NonCommercial-NoDerivatives License 4.0

<sup>1</sup>To whom correspondence may be addressed. Email: zhangmj@sustech.edu.cn.

This article contains supporting information online at https://www.pnas.org/lookup/suppl/doi:10.1073/pnas. 2417346122/-/DCSupplemental.

Published January 23, 2025.

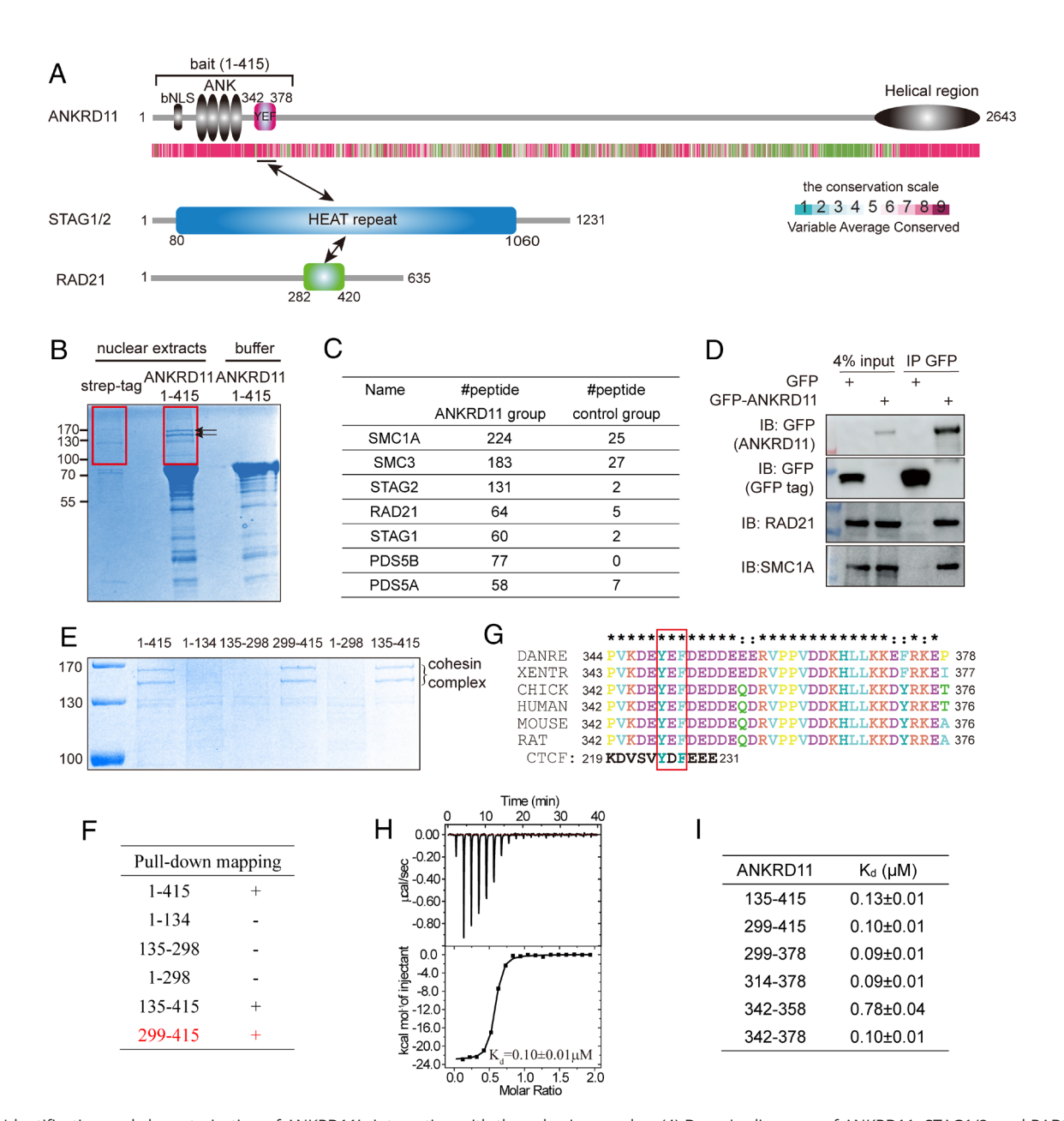


**Fig. 1.** Identification and characterization of ANKRD11's interaction with the cohesin complex. (*A*) Domain diagrams of ANKRD11, STAG1/2, and RAD21 with a vertebrate conservation heatmap below ANKRD11. bNLS: bipartite nuclear localization signal. (*B*) Coomassie Blue-stained gel of affinity-purified proteins from nuclear extracts using strep-tagged ANKRD11\_1-415 or strep tag alone. Red boxes indicate bands analyzed by mass spectrometry. Black arrows indicate the protein bands specifically pulled down by ANKRD11\_1-415. (*C*) Mass spectrometry results showing peptide counts of the cohesin complex subunits pulled down by ANKRD11\_1-415. (*D*) Coimmunoprecipitation (Co-IP) assay demonstrating the interaction between overexpressed GFP-ANKRD11 and the endogenous cohesin complex components (SMC1A and RAD21). (*E*) Sodium dodecyl sulfate-polyacrylamide gel electrophoresis (SDS-PAGE) analysis of the cohesin complex pull-down using various truncated ANKRD11 fragments. (*F*) Summary of the pull-down mapping results in panel *E*. (*G*) Multiple sequence alignment of the conserved YEF motif in ANKRD11 across species. The YDF motif from CTCF is also included in the analysis. (*H*) Representative ITC curve showing the interaction between ANKRD11\_342-378 and the STAG2-RAD21 complex. (*I*) Table summarizing the dissociation constants (K<sub>d</sub>) of various ANKRD11 truncations binding to the STAG2-RAD21 complex determined by ITC.

The cohesin complex, which includes the Adenosine Triphosphate (ATP)-dependent ATPase core subunits Smc1, Smc3, Scc1 (RAD21), and Scc3 (STAG1/STAG2), plays a critical role in sister chromatid cohesion, DNA damage repair, and the regulation of three-dimensional (3D) genome folding and gene expression (24–29). Through its loop extrusion activity, cohesin and CCCTC-binding factor (CTCF) collaboratively organize the 3D structure of the genome and regulate gene expression by forming chromatin loops and topologically associating domains (TADs), which is essential for enhancer–promoter (E-P) interactions in gene transcriptions (30–33). In the context of CdLS, mutations in cohesin or its loader NIPBL, which also activates cohesin's ATPase activity for loop extrusion (34, 35), lead to a broad dysregulation of gene

expression, without sister chromatid cohesion defect (30, 36, 37). Non-cohesin-complex protein BRD4 has been reported to interact with NIPBL and stabilize NIPBL on chromatin, thereby influencing genome folding and loop extrusion critical for neural crest progenitor differentiation (15, 38, 39). However, the relationship between ANKRD11 and cohesin remains largely unexplored.

In this study, we find that ANKRD11 directly interacts with the cohesin complex. Structural studies reveal that ANKRD11 binds to the STAG2–RAD21 subcomplex through an extended "YEF" motif—containing fragment with high affinity and specificity. We demonstrate that disruption of the ANKRD11 and cohesin interaction alters gene expression in mouse embryonic stem cells (mESCs). In mice, disruption of the interaction between

ANKRD11 and cohesin causes a loss of the interfrontal bone as well as autism-like behavior. Our study establishes a mechanistic link between ANKRD11 and the cohesin complex and explains why ANKRD11 plays critical roles in the nervous system and craniofacial development in mammals including humans.

#### Results

Identification of the Cohesin Complex as a Specific Binder of ANKRD11. To investigate the underlying mechanism of ANKRD11's function in development and its role in disease pathogenesis, we employed affinity purification coupled with mass spectrometry (AP-MS) method employing Strep-tagged fragments of ANKRD11 to identify its potential interacting proteins. Utilizing N-terminal fragments of ANKRD11 (amino acids 1 to 415, encompassing the conserved region in the N-terminal region) as the bait (Fig. 1A) and nuclear extracts from HeLa cells as the source of potential interactors, two prominent protein bands were specifically pulled down (Fig. 1B). Mass spectrometry analysis identified the two bands as subunits of the cohesin complex (Fig. 1C). In contrast, Strep tag alone exhibited minimal or no affinity for the cohesin subunits (Fig. 1 B and C), indicating a specific interaction between ANKRD11 and the cohesin complex in HeLa cells. Consistent with our findings, a previous proteomic study using SMC1A as the bait also identified ANKRD11 as a potential interacting partner of the cohesin complex (40). Notably, SMC1A, SMC3, RAD21, STAG1/2, and PSD5A/B are highly enriched in our purification. Curiously, CTCF, known to bind to the cohesin complex with submicromolar affinity (41), was not present in the affinity-purified cohesin complex. To confirm the interaction between ANKRD11 and the cohesin complex, we performed Coimmunoprecipitation (Co-IP) assays in HeLa cells transfected with Green Fluorescent Protein (GFP)-tagged ANKRD11. As expected, the cohesin complex subunits SMC1A and RAD21 specifically coimmunoprecipitated with GFP-ANKRD11 (Fig. 1*D*). The above results suggest that ANKRD11 forms a complex with the cohesin complex.

ANKRD11 Binds to the STAG2-RAD21 Subcomplex of Cohesin through a Conserved YEF Motif-Containing Fragment. Next, we studied the molecular mechanism underlying the ANKRD11 and cohesin interaction. We first used the affinity purification assay described above to map the minimal region of ANKRD11 responsible for binding to cohesin. We divided the N-terminal region into several segments: the N-terminal disordered region containing two NLS sequences (1 to 135), the middle ankyrin repeat (135 to 298), and the C-terminal disordered region (299 to 415), and two combined regions consisting of 2 to 298 and 135 to 415. Pull-down experiments showed that only protein fragments containing the C-terminal disordered region specifically bind to the cohesin complex, indicating that the 299 to 415 region contains the cohesin-binding site of ANKRD11 (Fig. 1 E and F). Further sequence analysis of this region revealed a highly conserved YEF motif-containing peptide fragment in this region, which resembles the "YDF" motif in CTCF known for its role in cohesin binding (Fig. 1G) (41), suggesting that ANKRD11 may interact with the cohesin complex via the YEF motif-containing fragment.

To test this possibility, we purified various lengths of ANKRD11 fragments containing the YEF motif and measured their bindings to the purified STAG2-RAD21 subcomplex of cohesin, which is known to mediate the interaction between CTCF and cohesin (41) using isothermal titration calorimetry (ITC). We found that ANKRD11 fragments containing the YEF motif fragment shown

in panel G (i.e., residues 342 to 378 based on the human ANKRD11 sequence) bind to the STAG2-RAD21 subcomplex with a  $K_d \sim 0.1$ μM (Fig. 1 H and I). Further truncations of the 342 to 378 fragment caused reduced bindings to the STAG2-RAD21 subcomplex (Fig. 11 and SI Appendix, Fig. S2). Thus, the 342 to 378 segment is the minimal sequence responsible for ANKRD11 to bind to cohesin. Sequence alignment indicated that ANKRD11 uses a longer peptide fragment than the CTCF YDF-motif peptide in binding to cohesin (Fig. 1*G*). Moreover, ANKRD12, a paralog of ANKRD11 containing a similar YEF motif, also binds to cohesin with  $K_d \sim 0.3 \mu M$  (SI Appendix, Fig. S3).

Structural Basis for ANKRD11-Cohesin Interaction. To understand the molecular basis governing the ANKRD11/cohesin complex interaction, we solved the crystal structure of the ANKRD11\_342-378/STAG2-RAD21 tripartite complex at 3.2 Å resolution (SI Appendix, Table S1). ANKRD11 employs a binding mechanism similar to that of CTCF and SGO1, with the ANKRD11 peptide anchoring to the conserved essential surface formed in the STAG2 and RAD21 interface (Fig. 2A) (41, 42). We have divided the binding interface into three sites: Site 1 encompasses the hydrophobic interactions involving the YEF-motif; site 2 is characterized by electrostatic interactions between the negatively charged residues following the YEF-motif of ANKRD11 and positively charged residues from the STAG2-RAD21 subcomplex; and site 3 is a binding site specific to the ANKRD11-cohesin complex and involves the extended and positively charged tail of ANKRD11\_342-378 (Fig. 2 B and C).

At site 1, Y347 and F349 from ANKRD11 anchor into two hydrophobic pockets of the STAG2-RAD21 subcomplex (Fig. 2D), and this binding mode is highly similar to that of the YDF-motif from CTCF or SGO1. To validate the interactions in site 1, we substituted Y347 and F349 in ANKRD11, or W334, F367, and F371 in STAG2, as well as I337 and L341 in RAD21 individually with Ala. ITC and pull-down assays showed that each of these mutations either completely abolished or significantly reduced the binding (Fig. 2H and SI Appendix, Figs. S4 A-E and S5). In particular, the substitution of either Y347 or F349 with Ala resulted in complete disruption of the interaction between ANKRD11 and the STAG2-RAD21 subcomplex (Fig. 2 H and I and SI Appendix, Fig. S4A). This analysis allowed us to create a single amino acid residue substitution (the Y347A mutant) within the giant ANKRD11 (a total of 2,643 aa) to completely disrupt the ANKRD11-cohesin interaction for functional studies described later in this study. At site 2, a stretch of negatively charged residues engage in charge-charge interactions with R298 and H295, and form hydrogen bonds with Y297 and Y331 in STAG2 (Fig. 2E). Mutations of either R298 or Y297 to alanine significantly weakened the binding, as shown by ITC and pulldown assays (Fig. 2H and SI Appendix, Figs. S4G and S5). Site 3 primarily consists of hydrogen bonds formed by D362 and D363 of ANKRD11 and Q140 and N141 of STAG2, as well as hydrogen bonds between D198 and S202 of STAG2 and the main chain of ANKRD11 (Fig. 2F). Deletion of residues from the site 3 region of ANKRD11 or mutations of either N141 or S202 of STAG2 to Ala all weakened the binding (Fig. 2*G* and *SI Appendix*, Figs. S4 H and I and S5). Charge potential analysis showed that STAG2 contains a negatively charged pocket in the site 3 region, which is favorable for interacting with a stretch of positively charged residues at the tail of ANKRD11\_342-378 (Fig. 2 C and G). Deletion of the positively charged residues of ANKRD11\_342-378 indeed weakened its binding to cohesin (SI Appendix, Fig. S41). In summary, the ANKRD11-cohesin complex structure and the biochemical analysis corroborate our

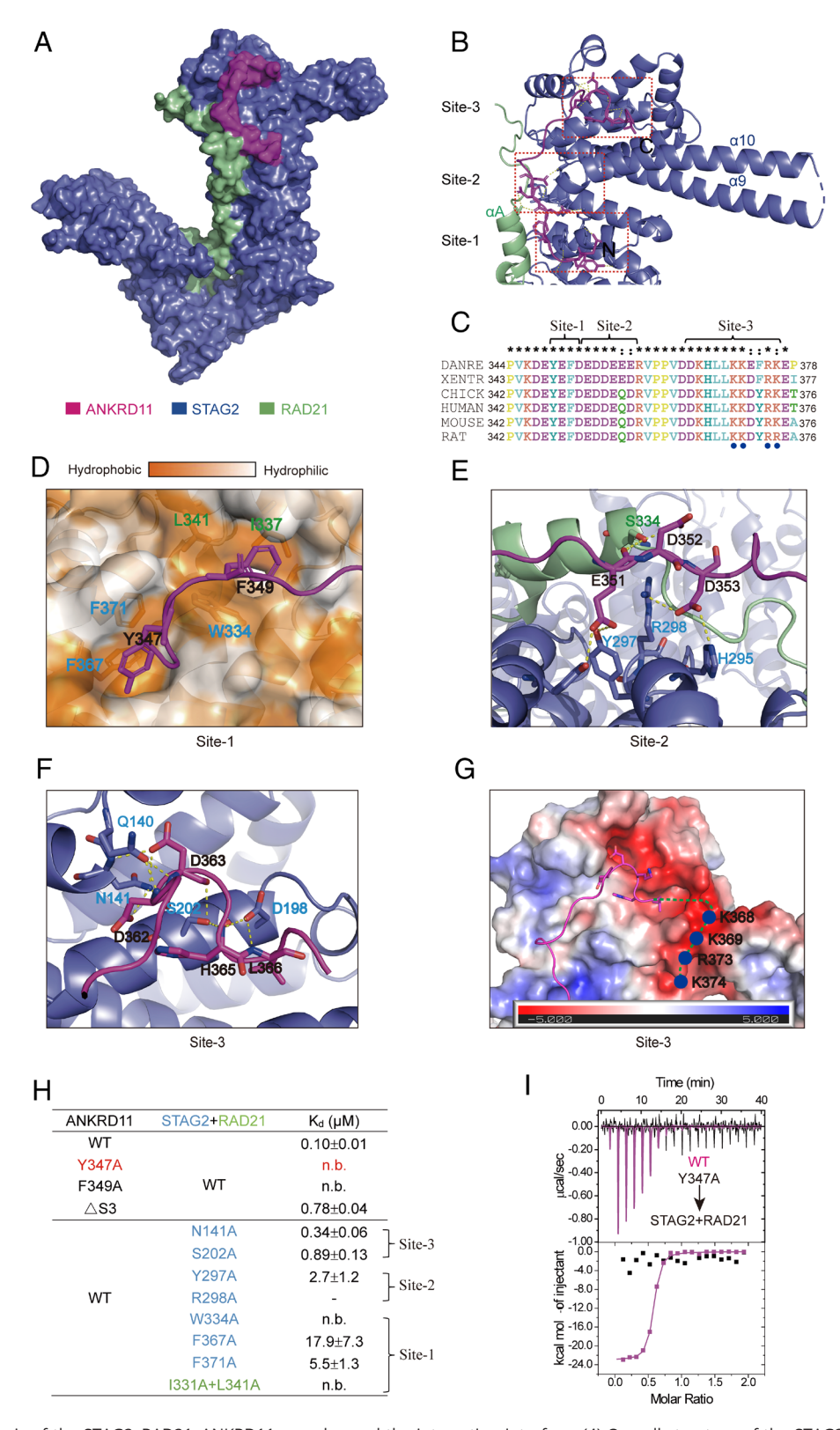


**Fig. 2.** Structural analysis of the STAG2–RAD21–ANKRD11 complex and the interaction interface. (*A*) Overall structure of the STAG2–RAD21 complex bound to ANKRD11 rendered with the surface model. The coloring scheme is shown in the cartoon diagram and the scheme is used throughout the paper. (*B*) The ANKRD11/STAG2–RAD21 interface is divided into three regions: site 1, site 2, and site 3. (*C*) Multiple sequence alignment of ANKRD11 across species, highlighting the conserved residues at the three binding sites. (*D*–*P*) Detailed views of the molecular interactions at site 1 (*D*), site 2 (*E*), and site 3 (*F*) of the ANKRD11/STAG2–RAD21 interface. (*G*) Electrostatic surface potential of STAG2 at site 3, calculated using Adaptive Poisson-Boltzmann Solver (APBS) in PyMOL. Positively charged ANKRD11 residues (blue circles) and their potential interactions with the negatively charged STAG2 pocket are indicated. (*H*) Table summarizing the dissociation constants (*K*<sub>d</sub>) determined by ITC for wild-type (WT) and mutant ANKRD11 peptides binding to the STAG2–RAD21 complex. n.b.: no binding. The raw ITC data are shown in *Sl Appendix*, Fig. S4. (*l*) Representative ITC curves comparing the binding of WT ANKRD11 and the Y347A mutant to the STAG2–RAD21 complex, showing that the mutant had no detectable binding to cohesion.

prior mapping results showing that ANKRD11 used an extended "YEF" motif to interact with the cohesin complex.

ANKRD11 Effectively Competes with CTCF for Cohesin Binding. Through comparison of the CTCF/cohesin and ANKRD11/ cohesin complex structures, it is evident that ANKRD11 and CTCF bind to cohesin with a similar mode, albeit that the ANKRD11 peptide occupies a longer groove in the STAG2-RAD21 subcomplex (Fig. 3 A and B). Consistent with this structural analysis, the ANKRD11 peptide binds to the STAG2-RAD21 subcomplex with a ~fourfold higher affinity than the CTCF peptide does (Fig. 3C;  $K_d$  values of 0.1  $\mu M$  vs. 0.4  $\mu M).$ This analysis predicted that the bindings of ANKRD11 and CTCF to cohesin are mutually exclusive and ANKRD11 should be able to effectively compete with CTCF in binding to cohesin. A competition experiment indeed showed that ANKRD11 effectively outcompeted CTCF in binding to the STAG2-RAD21 subcomplex (Fig. 3D). Specifically, more than 50% of the CTCF/ cohesin complex was disrupted when an equimolar amount of ANKRD11 and CTCF were mixed with the STAG2-RAD21 subcomplex, and the majority of the CTCF/cohesin complex dissociated when a two-molar ratio of ANKRD11 was added to compete with CTCF. The above result explains why CTCF was absent in the affinity-purified cohesin complex in Fig. 1B.

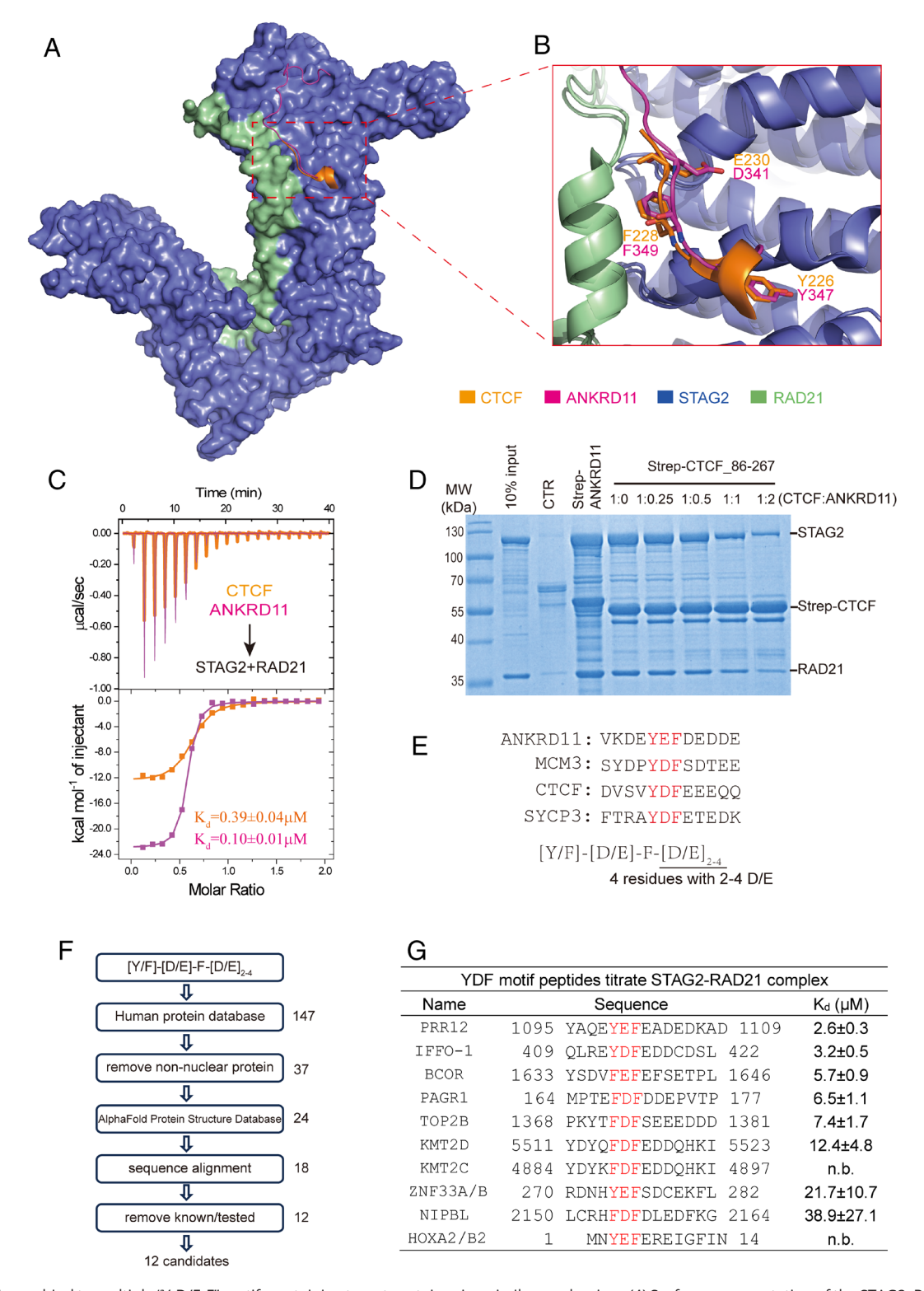
Identification of Additional Cohesin Ligands. Our structural and biochemical analyses, together with earlier studies of the interaction between CTCF and cohesin (41), revealed that the strong cohesin binders possess 2 to 4 negatively charged amino acids following the Y-[DE]-F motif (i.e., [Y/F]-[D/E]-F-[D/E]<sub>2-4</sub>) (Fig. 3E). To identify additional potential cohesin binders, we searched human protein databases using this consensus motif. The initial search yielded 147 proteins. We excluded non-nuclear proteins, proteins with identified motifs inaccessible for binding due to protein folding, and candidates with identified motifs that are not evolutionary conserved (Fig. 3F). This stringent selection process resulted in 18 potential binders, including five known cohesin binders (ANKRD11/12 characterized in this study, CTCF, Minichromosome Maintenance Complex Component 3, and Synaptonemal Complex Protein 3 identified previously (41, 43). We then removed the known or previously tested ones (Cadherin 6) and synthesized 10 peptides containing the [Y/F]-[D/E]-F-[D/ E]<sub>2-4</sub> motif of each of these final candidate proteins and used ITC to test their bindings to cohesin. Remarkably, 9 out of these 12 peptides were found to bind to cohesin. Among them, the peptide fragment from Proline Rich 12 (PRR12) showed the strongest binding (Fig. 3G and SI Appendix, Fig. S6). Fittingly, PRR12 was recently identified as a cohesin regulator through coessentiality analysis and AP-MS experiments, though the direct binding between PRR12 and cohesin was not investigated (44). Another cohesin binder PR domain-containing GTPase activating protein 1 (PAGR1) was recently implicated to regulate cohesin's association with chromatin thereby influencing transcription and DNA repair processes (45, 46). Both PRR12 and PAGR1, like ANKRD11, are transcriptional regulators engaged in chromatin organization and neuronal development (47-49). It remains to be tested whether the rest of the six identified proteins (Intermediate Filament Family Orphan 1, BCL6 Corepressor, DNA topoisomerase 2-beta, Lysine Methyltransferase 2D, and Zinc Finger Protein 33A/B) are cohesin binders under physiological conditions.

Y347A Mutation Disrupts the Interaction between the Full-**Length ANKRD11 and Cohesion.** We next investigated whether the identified cohesin-binding site spanning residues 342-378 represents

the only cohesin-binding site of ANKRD11. We overexpressed GFP-tagged full-length ANKRD11, both the wild-type (WT) and the Y347A mutant, in HeLa cells and conducted pull-down assays. GFP-tagged WT ANKRD11 pulled down various subunits of the endogenous cohesin complex (Fig. 4A), indicating that the full-length ANKRD11 can specifically interact with cohesin. Again, CTCF was not detected in the WT ANKRD11 pull-down experiment (Fig. 4A), suggesting that CTCF was competed off from the cohesin complex by ANKRD11. Importantly, the Y347A mutation completely disrupted the interaction between ANKRD11 and the cohesin complex (Fig. 4A), confirming that the 342 to 378 segment is the only cohesin-binding region of ANKRD11. Since Y347 is situated in an unstructured region of ANKRD11 (Fig. 1A), the single residue substitution Y347A should not alter the structure and interactions of the giant ANKRD11 with any target proteins other than cohesin. Thus, the ANKRD11\_Y347A mutant is uniquely suited to investigate the function of the interaction between ANKRD11 cohesin as described below.

We next asked whether endogenous ANKRD11 indeed binds to cohesin. This is critical since cohesin has multiple potential binding targets (Fig. 3), in addition to the well-established target CTCF. Neither commercially available nor our home-made antibodies against ANKRD11 worked well for immunoprecipitation experiments. To overcome this challenge, we employed CRISPR-Cas9 technology to knock in a Flag-Avi tag at the N-terminal of ANKRD11 in mESCs (Fig. 4B and SI Appendix, Fig. S7 A and B), so that the endogenous ANKRD11 can be labeled with biotin. We then used another round of CRISPR-Cas9 gene editing to introduce a Y347A mutation to ANKRD11 (Fig. 4C and SI Appendix, Fig. S7 C and D). For in vivo biotinylation of the Avi tag, the Flag-Avi tagged ANKRD11 cells were infected with the lenti-birAV5 lentivirus to overexpress the BirA enzyme (SI Appendix, Fig. S7 E and F) (50). Immunoprecipitation results showed that WT ANKRD11 coimmunoprecipitated the cohesin complex, albeit with a lower amount than in the GFP-ANKRD11 overexpressing cells (Fig. 4D). The ANKRD11-bound cohesin complex does not contain CTCF. The Y347A mutation completely disrupted the interaction between ANKRD11 and cohesin (Fig. 4D). These findings demonstrate that endogenous ANKRD11 is associated with cohesin, and the interaction can be effectively disrupted by substituting the single residue Y347 with Ala.

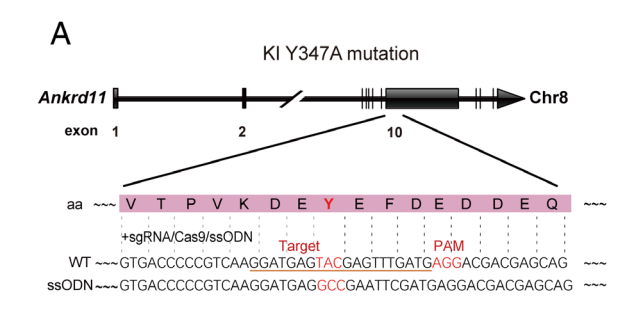
The ANKRD11-Cohesin Interaction Regulates Gene Expressions Related to Neural Development. Given the critical roles of both ANKRD11 and the cohesin complex in development and the overlapping phenotypes arising from their mutations, we hypothesized that their interaction might have significant biological functions. To validate this hypothesis, we first performed Western blot analysis and found that the ANKRD11 protein levels were not significantly different between WT and Y347A mutant mESCs (SIAppendix, Fig. S7 G and H), indicating that the Y347A mutation does not alter ANKRD11 expression. With this confirmation, we proceeded to evaluate the impact of the Y347A mutation on the pluripotency of mESCs. The Y347A mutant clones exhibited normal morphology and proliferation compared to the WT clones (SI Appendix, Fig. S8 A and B). Alkaline Phosphatase staining assay indicated that the Y347A mutant clones retained pluripotency (SI Appendix, Fig. S8C). Nonetheless, RT-qPCR analysis showed a slight downregulation of pluripotency markers Sox2 and Nanog, but Oct4 expression remained unchanged, suggesting a subtle tendency toward pluripotency exit caused by the mutant. To further explore the impact of the Y347A mutation, we performed RNA sequencing (RNA-seq) of WT and Y347A mutant mESC clones. Correlation analysis and principal component analysis revealed that

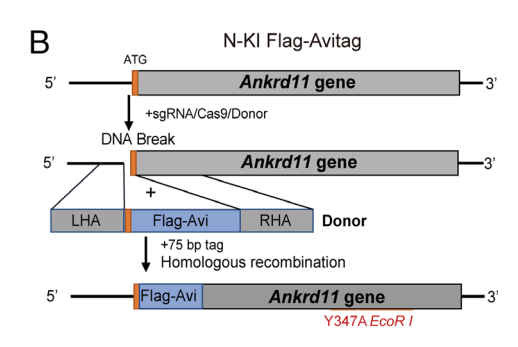


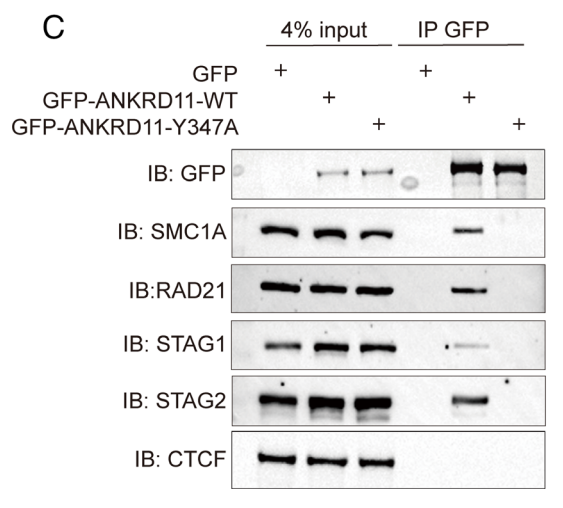
**Fig. 3.** Cohesin can bind to multiple "Y-D/E-F" motif-containing target proteins via a similar mechanism. (*A*) Surface representation of the STAG2-RAD21 complex with bound CTCF and ANKRD11 peptides overlayed with each other. (*B*) Zoomed-in view of the binding interface, highlighting key residues involved in the bindings. (*C*) ITC curves showing the bindings of ANKRD11 and CTCF peptides to the STAG2-RAD21 complex with  $K_d$  values for ANKRD11 (0.10 ± 0.01 μM) and for CTCF (0.39 ± 0.04 μM) indicated. (*D*) SDS-PAGE analysis of the competition assay between ANKRD11 (342 to 378) and Strep-tagged CTCF for binding to the STAG2-RAD21 complex with increasing molar ratios of ANKRD11 to CTCF included in the assay. (*E*) Sequence alignment of known strong cohesin binders, revealing the consensus "[Y/F]-[D/E]-E-[D/E]-E-" motif for binding to cohesin. (*P*) Flowchart depicting the database search process to identify potential cohesin-binding proteins containing the "[Y/F]-[D/E]-E-[D/E]-E-" motif. (*G*) Table summarizing the dissociation constants (E-) for peptides containing the "[Y/F]-[D/E]-E-[D/E]-E-" motif binding to the STAG2-RAD21 complex. The sequences of the peptides are shown with the core motif highlighted in red. n.b.: no binding.

biological replicates within each group (WT and Y347A mutant) were highly correlated and clustered closely together (*SI Appendix*, Fig. S8 *E* and *F*). Differential gene expression analysis showed that the ANKRD11 Y347A mutation led to the upregulation of

1,318 genes and the downregulation of 1,137 genes (*SI Appendix*, Fig. S8*G*). Gene set enrichment analysis indicated no significant enrichment of the "Mouse Embryonic Stem Cell Pluripotency Genes" set, supporting the observation that the overall pluripotency







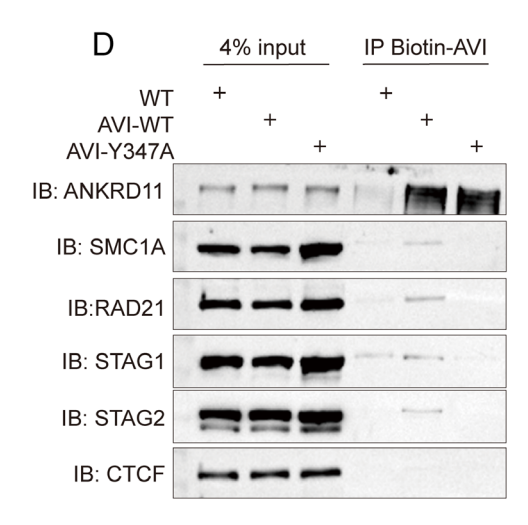


Fig. 4. The Y347A mutation in ANKRD11 disrupts both exogenous and endogenous ANKRD11-cohesin interactions. (A) Co-IP of GFP-WT or Y347A ANKRD11 with endogenous cohesin subunits and CTCF. Immunoblotting for indicated proteins. (B) Schematic representation of CRISPR/Cas9-mediated knock-in strategy for inserting a Flag-Avi tag at the N terminus of the ANKRD11 gene in mESCs. LHA: left homology arm; RHA: right homology arm. (C) Schematic illustration of CRISPR/Cas9-mediated knock-in strategy for introducing the Y347A mutation in the ANKRD11 gene in mESCs. The sgRNA targeting sequence, Y347A mutation site, and introduced restriction enzyme site are underlined. Mutated base and PAM sequence are highlighted in red. The amino acid (aa) sequence surrounding the mutation site is shown in the pink box. (D) Co-IP analysis of endogenous Avi-tagged ANKRD11 (WT or Y347A) with endogenous cohesin subunits and CTCF in mESCs.

was largely maintained in Y347A mutants (SI Appendix, Fig. S8H). The differentially expressed genes (DEGs) were enriched in neuralrelated pathways: Down-regulated genes were associated with cell morphogenesis, regulation of nervous system development, and brain development (Fig. 5A), up-regulated genes were involved in response to wounding and negative regulation of nervous system development pathways (Fig. 5B), suggesting that the Y347A mutation may impact neural development processes.

Next, to further investigate the relationship between ANKRD11 and cohesin function, we analyzed the overlaps between deregulated genes in ANKRD11 Y347A mutants (this study) and genes deregulated by the RAD21 depletion using RNA-seq data from a published study (GSE178982) generated from the auxin-inducible degradation of the cohesin subunit RAD21 in mESC (51). Despite different mESC culture conditions, there was a significant overlap in the gene sets elicited by ANKRD11 Y347A mutation and the 24-h degradation of RAD21, the up-regulated gene sets in particular (Fig. 5 C and D). This indicates that gene expression changes caused by the Y347A mutation are likely connected to the loss of its binding to the cohesin complex. These co-down-regulated genes are primarily associated with nucleosome assembly (Nasp, H1f1, H3c3, H2ac11, etc.), negative regulation of neurogenesis (Ifrd1, Sox11, Lin28a, Arhgap4, etc.), and skeletal system development (Actn3, Cited2, Sox11, Msc, etc.) (Fig. 5 *E* and *F*). The co-up-regulated genes by the ANKRD11 Y347A mutation and RAD21 degradation are also related to the regulation of neurogenesis (Ece1, Ephb2, Gata2, Scn1b, etc.) and bone development

(Matn1, Msx2, Npr2, Bmp7, etc.), as well as the neuron apoptotic process (Btg2, Clu, Crlf1, Trp73, etc.) and wound healing pathways (Anxa2, Anxa5, Cadm4, Cldn4, etc.) (Fig. 5 G and H). These results indicate that the interaction between ANKRD11 and cohesin is involved in pathways related to neural and bone development, and defects in this interaction may cause neuronal and craniofacial development abnormalities as seen in KBG syndrome and CdLS.

ANKRD11 Y347A Mutation Affects Mouse Neural and Craniofacial **Development.** To investigate the function of the ANKRD11– cohesin interaction, we generated Y347A mutant mice using the CRISPR-Cas9 technology (SI Appendix, Fig. S9 A and B). The most characteristic pathological manifestation of KBG syndrome is the abnormal development of craniofacial bones and neural developmental delay (1, 2). To determine whether the ANKRD11\_ Y347A mutation affects skeletal morphology, we conducted X-ray imaging of the whole body and the skull in the homozygous mutant  $(ANKRD11^{mut/mut})$  and WT  $(ANKRD11^{WT/WT})$  mice. The images revealed no significant skeletal abnormalities in the ANKRD11 Y347A mutants compared to WT controls (SI Appendix, Fig. S9C). Additionally, growth monitoring from 3 to 12 wk of age showed that both male and female homozygous ANKRD11\_Y347A mice displayed normal growth patterns and had similar body weights compared to their WT littermates, indicating that the mutation does not affect overall growth and development through to adulthood (SI Appendix, Fig. S9D).

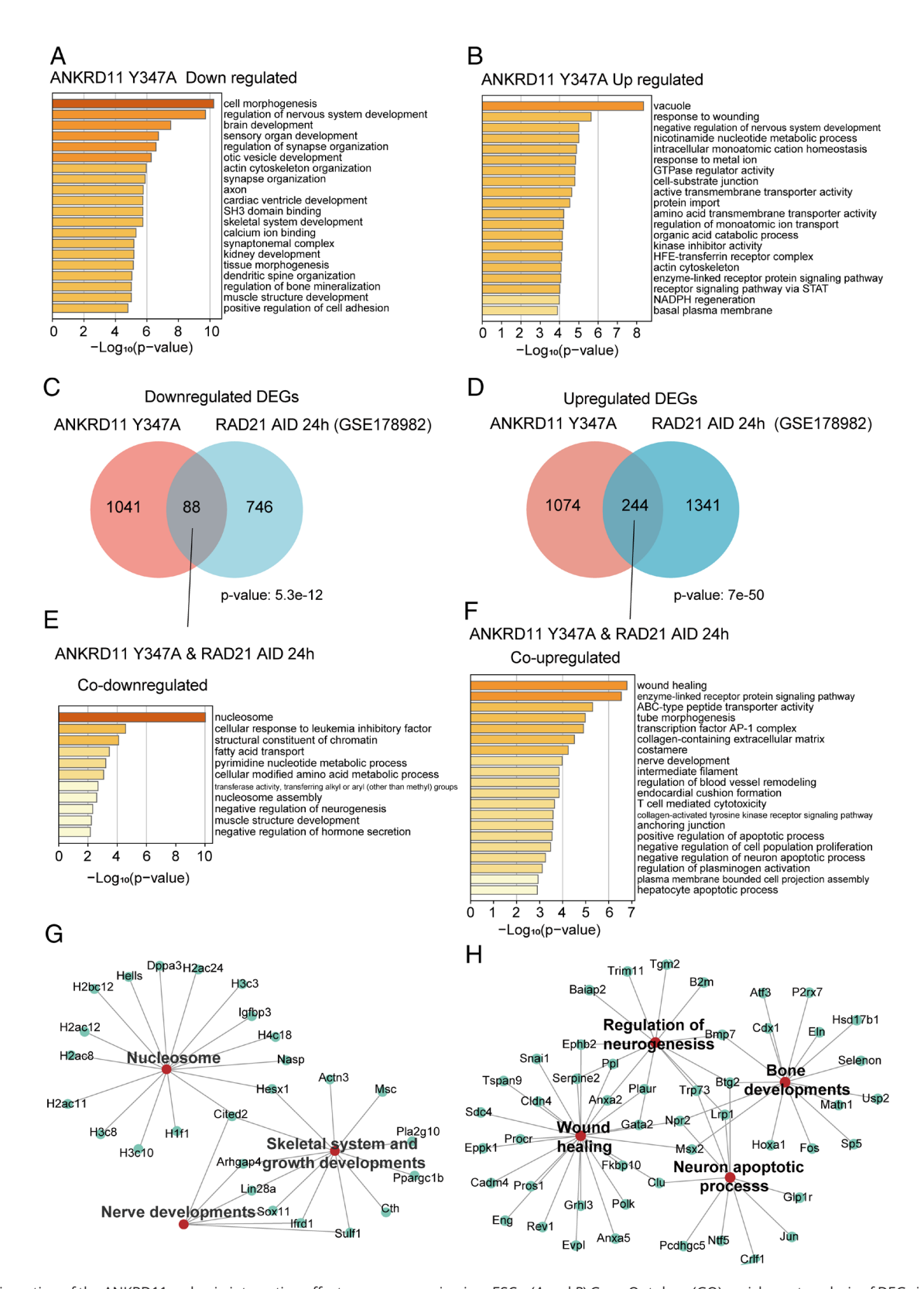


**Fig. 5.** Disruption of the ANKRD11-cohesin interaction affects gene expression in mESCs. (*A* and *B*) Gene Ontology (GO) enrichment analysis of DEGs in ANKRD11 Y347A mutant mESCs. (*A*) Down-regulated and (*B*) up-regulated DEGs. (*C* and *D*) Venn diagrams showing the overlap of DEGs caused by the ANKRD11 Y347A mutation and by RAD21 depletion. (*C*) Down-regulated and (*D*) up-regulated DEGs. *P*-value by the hypergeometric test. (*E* and *F*) Analysis of genes co-down-regulated in both ANKRD11 Y347A mutant and RAD21-depleted cells. (*F*) GO enrichment analysis. (*F*) Network visualization of key GO functional categories. (*G* and *H*) Analysis of genes co-up-regulated in both ANKRD11 Y347A mutant and RAD21-depleted cells. (*G*) GO enrichment analysis. (*H*) Network visualization of key GO functional categories.

For the craniofacial development study, we utilized micro-computed tomography (micro-CT) scans and found that the interfrontal bone present in WT mice was missing in the majority of

ANKRD11 Y347A mutant mice, replaced instead by a single interfrontal suture (Fig. 6 *A* and *B*). A subset of mutant mice retained the interfrontal bone, albeit with a significantly reduced area

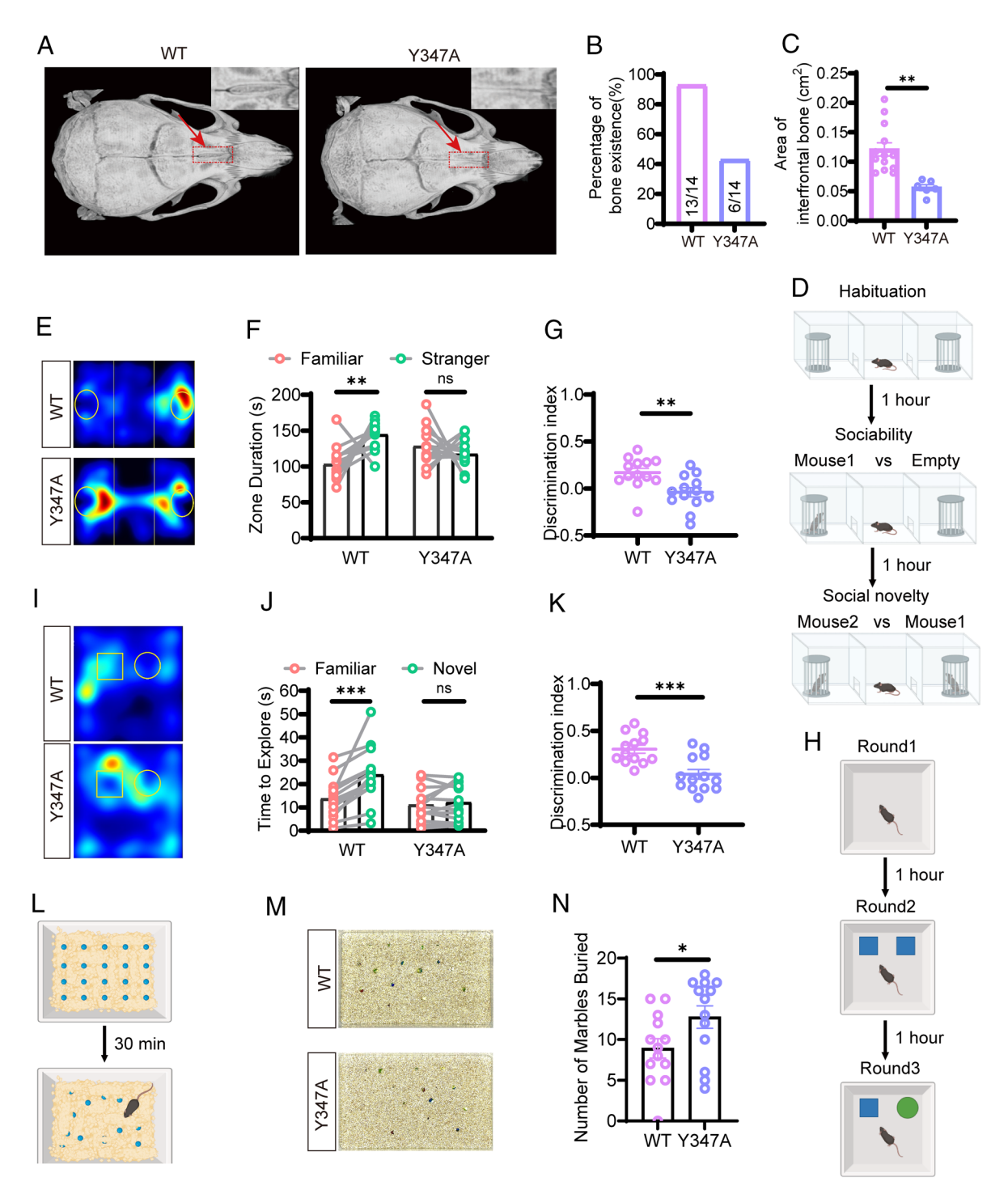


Fig. 6. Disruption of the ANKRD11-cohesin interaction affects craniofacial development and social behavior in mice. (A) Micro-CT scans of craniofacial structures in WT and Y347A mutant mice. Red arrows/outlines highlight the interfrontal bone region with magnified insets. (B) Quantification of interfrontal bone existence in WT and Y347A mice. The percentage of mice with the interfrontal bone present is significantly reduced in the Y347A group compared to the WT group (WT: 13/14; Y347A: 6/14). (C) Quantitative analysis of the interfrontal bone area in WT and Y347A group. The interfrontal bone area was significantly reduced in the Y347A group compared to the WT group, as shown by the mean values ± SEM. Statistical significance was determined using an unpaired t test [\*\*P < 0.01; N = 13 (WT); 6 (Y347A)]. (D) Schematic of the three-chamber social interaction test protocol. (E) Representative heat maps showing exploration patterns of WT and Y347A mice during the social novelty phase (Familiar Mouse vs. Novel Mouse) of the three-chamber test. (F) Quantification of time spent in zones containing familiar or novel mice during the social novelty phase (Mouse2 vs. Mouse1) for WT and Y347A groups. Data are mean ± SEM (n = 13 per group). \*\*P < 0.01; paired t test. (G) Discrimination index for the social novelty phase. Individual data points and mean ± SEM are shown (n = 13 per group). \*\*P < 0.01; unpaired t test. (H) Schematic of the novel object recognition test protocol. (I) Representative heat maps showing exploration patterns of WT and Y347A mice during the test phase (Round 3) of the novel object recognition task. (/) Time spent exploring familiar and novel objects during the test phase for WT and Y347A groups. Data are mean ± SEM (n = 13 per group). \*\*\*P < 0.001; ns, not significant; paired t test. (K) Discrimination index for the novel object recognition test. Individual data points and mean ± SEM are shown (n = 13 per group). \*\*\*P < 0.001; unpaired t test. (L) Schematic of the marble burying test protocol. (M) Representative images of the marble burying test for WT and Y347A mice. (N) Bar graphs showing the number of marbles buried by WT and Y347A mice. Data are mean ± SEM (n = 13 per group). \*P < 0.05; unpaired t test.

compared to the WT group. (Fig. 6C). Notably, the presence of an interfrontal bone varies across mouse strains (52). For example, C57BL/6J mice typically exhibit an interfrontal bone, whereas it is absent in C3H/HeJ mice. Yoda mice, a subset of the C3H/HeJ strain carrying a heterozygous Ankrd11 missense mutation, also exhibit an unfused interfrontal suture (23). In our experiments with the C57BL/6J strain, the transition from an interfrontal bone to an interfrontal suture in the Y347A mutant mice mirrored the phenotype observed in Yoda mice.

Given the prevalence of social and cognitive impairments in KBG syndrome patients, we investigated potential behavioral phenotypes in ANKRD11\_Y347A mutant mice. We employed three-chamber social interaction tests and novel object recognition tasks to assess social behavior and cognitive function, respectively (Fig. 6 D and H). In the three-chamber social interaction test, both WT and mutant mice showed no location preference during the habituation phase (SI Appendix, Fig. S10 A-C). In the sociability, both groups exhibited significant social preferences toward unfamiliar mice, indicating intact initial social motivation (SI Appendix, Fig. S10 *D–F*). However, in the social novelty, ANKRD11\_Y347A mutant mice displayed equal social tendencies toward unfamiliar and familiar mice, while WT mice maintained a preference for unfamiliar mice. This difference was quantified by discrimination indices of 24.6% for WT and -5.8% for ANKRD11\_Y347A mutant mice (Fig. 6 E-G), suggesting a specific deficit in social novelty recognition in mutant mice. We assayed general locomotor activities of the WT and Y347A mice and found that the mutation did not alter the locomotor activity of the mice (*SI Appendix*, Fig. S10 *J* and *K*).

To assess cognitive function, we utilized the novel object recognition test (Fig. 6H). During habituation, both WT and ANKRD11 Y347A mutant mice showed equal interest in two identical objects (SI Appendix, Fig. S10 G-I). In the test phase, WT mice exhibited a clear preference for the novel object, whereas mutant mice showed no preference between new and familiar objects. This cognitive difference was reflected in discrimination indices of 35.2% for WT mice and 3.7% for ANKRD11 Y347A mutant mice (Fig. 6 I-K). These findings indicate that the ANKRD11 Y347A mutation impairs recognition memory. Additionally, to assess repetitive and compulsive behaviors in ANKRD11 Y347A mutant mice, we conducted a marble burying test. Twenty marbles were evenly distributed on the cage surface, and the number of buried marbles was counted after 30 min (Fig. 6L). Y347A mutant mice exhibited significantly enhanced burying behavior compared to WT controls (Fig. 6 L-N). This increased marble burying behavior indicates a heightened tendency toward repetitive and compulsive behaviors in Y347A mice, mirroring the autism and obsessive-compulsive symptoms commonly observed in KBG syndrome patients (53, 54).

Taken together, the above skull development and the behavioral studies collectively indicate that the developmental abnormalities found in ANKRD11 Y347A mutant mice are correlated with the disrupted interaction of the protein with cohesin complex. The phenotypes of the ANKRD11 Y347A mutant recapitulate key aspects of KBG syndrome observed in patients.

### **Discussion**

The central findings of this study are the identification of a direct and specific interaction between ANKRD11 and the cohesin complex, and ANKRD11 competes with CTCF for binding to the cohesin complex. Our findings provide direct evidence showing why mutations in ANKRD11 and the cohesin complex share overlapping clinical phenotypes. Given that the cohesin complex, via interacting with CTCF, is a master regulator of chromatin

organization and gene transcription regulations (30, 55-57), it is not surprising that disruption of the ANKRD11-cohesin interaction (e.g., the Y347A mutation described in this study) can alter the ANKRD11-mediated gene expressions and cause developmental abnormalities in organs/tissues such as the brain and bones.

Our results can also rationalize why mutations in ANKRD11 and the cohesin complex display distinct phenotypes in patients. ANKRD11 is a very large protein with >2,600 amino acids. The region of ANKRD11 responsible for binding to the cohesin complex (i.e., aa 342 to 278 of ANKRD11) only occupies a very small portion of the protein that is unstructured. Thus, the majority of the ANKRD11 mutations found in patients (e.g., the mutationenriched C-terminal helical region, SI Appendix, Fig. S1) will not have a direct impact on the interaction between ANKRD11 and cohesin. Instead, some of these mutations likely affect the binding of ANKRD11 to the NCOR repressor complex. As an example, patients with heterozygous loss-of-function mutations of SETD5 present phenotypes that overlap with those observed in KBG syndrome (58, 59). Interestingly, KBG syndrome patients with SETD5 mutations have normal ANKRD11 (60, 61), suggesting a potential functional connection between ANKRD11 and SETD5. Indeed, both ANKRD11 and SETD5 can associate with the NCOR repressor complex (19, 62, 63).

Our study reveals that ANKRD11 Y347A mutation leads to specific deficits in craniofacial development and behavioral abnormalities in mice. When compared to other ANKRD11 mutant mouse models, Y347A mice show some overlapping yet distinct phenotypes. For example, Yoda mice, which carry a heterozygous ANKRD11 missense mutation, display an unfused interfrontal suture. In Y347A mice, the interfrontal bone is either completely absent and replaced by a suture or is reduced in size. While Yoda mice display broader craniofacial abnormalities including shortened snouts, wider skulls, and reduced bone mineral density, Y347A mice show relatively specific deficits limited to the interfrontal region without other significant skeletal abnormalities (23). The neural crest-specific *Ankrd11* deletions manifest more severe phenotypes, particularly in the homozygous state, including cleft palate, severe midfacial hypoplasia, and perinatal lethality (21). Behaviorally, both Y347A and Yoda mice exhibit social deficits and repetitive behaviors. Y347A mice show impaired social novelty recognition and increased marble burying, while Yoda mice display reduced social preference and more self-grooming (19). The above comparisons suggest that different mutations in ANKRD11 can result in varying degrees of severity in craniofacial and behavioral phenotypes, with our Y347A model indicating the importance of ANKRD11-cohesin interaction in craniofacial development and social behavior.

One key limitation of our study is that we have not fully elucidated how the ANKRD11-cohesin interaction influences gene expression at a deep mechanistic level. While we have demonstrated that disrupting this interaction leads to significant changes in gene expression patterns, the precise mechanisms by which ANKRD11 and cohesin collaborate to regulate transcription remain to be determined. To understand how ANKRD11 works with cohesin to regulate gene expression, it is important to consider the role of cohesin in orchestrating E-P interactions via loop extrusion. This process, together with CTCF, establishes TADs that can facilitate or restrict E-P contacts, thereby influencing gene expression patterns (30, 55). As a chromatin-associated protein, ANKRD11 can be found at the promoters of specific genes (19). During the cohesin-driven loop extrusion process, the encounter between cohesin and promoterbound ANKRD11 may lead to transient cohesin stalling. This stalling could enhance interactions between the promoter and distant enhancers or repressors, thus playing a crucial role in the regulation of gene transcription. This mechanism may also be used by other cohesin binders such as PRR12, which is a transcription regulator and important for development. We postulate that compared to CTCF, the level of ANKRD11 in cells of different tissues is much lower. Therefore, the ratio of the ANKRD11-bound cohesin to the CTCF-bound cohesin is likely to be low. If this postulation stands, the balance between ANKRD11 and CTCF protein levels will play important roles in ANKRD11-regulated gene expression in cells. It is likely that ANKRD11, in contrast to CTCF, may only regulate expressions of a small and specific set of genes. Consistent with this hypothesis, the phenotypic manifestations in patients caused by ANKRD11 mutations are much more specific than the CTCF/ cohesin mutations (10, 16, 64). Identifications of specific genes, of which the expressions are directly regulated by ANKRD11, are rather tricky. We tried conventional techniques such as RNA-Seq, chromatin immunoprecipitation sequencing, and Hi-C extensively and did not yield conclusive results. Nonetheless, our finding that the Y347A mutation in ANKRD11 specifically disrupts its interaction with the cohesin complex provides a good starting point for future mechanistic studies of the interaction between ANKRD11 and cohesin in gene expressions.

Another limitation of the current study is that we focused exclusively on homozygous Y347A mutants. Given that KBG syndrome is caused by heterozygous mutations in ANKRD11 in humans, it will be interesting to investigate whether heterozygous Y347A mice may display any anatomical and behavioral phenotypes.

#### **Materials and Methods**

Quantification, Statistical Analysis, and Data Availability. Animal behavior values are presented as mean  $\pm$  SEM. When normality and equal variance (F test) were met, unpaired or paired two-tailed Student's t tests were used, with

- 1. I. Parenti et al., ANKRD11 variants: KBG syndrome and beyond. Clin. Genet. 100, 187–200 (2021).
- A. Sirmaci et al., Mutations in cause KBG syndrome, characterized by intellectual disability, skeletal malformations, and macrodontia. Am. J. Hum. Genet. 89, 289-294 (2011).
- F. Brancati, A. Sarkozy, B. Dallapiccola, KBG syndrome. Orphanet J. Rare Dis. 12, 183 (2006).
- M. Isrie et al., Haploinsufficiency of ANKRD11 causes mild cognitive impairment, short stature and minor dysmorphisms. Eur. J. Hum. Genet. 20, 131-133 (2012).
- A. Goldenberg et al., Clinical and molecular findings in 39 patients with KBG syndrome caused by deletion or mutation of ANKRD11. Am. J. Med. Genet. A 170, 2847-2859 (2016).
- E. Martinez-Cayuelas et al., Clinical description, molecular delineation and genotype-phenotype correlation in 340 patients with KBG syndrome: Addition of 67 new patients. J. Med. Genet. 60, 644-654 (2023)
- C. W. Ockeloen et al., Further delineation of the KBG syndrome phenotype caused by ANKRD11 aberrations. Eur. J. Hum. Genet. 23, 1176-1185 (2015).
- A. Lo-Castro et al., Neurobehavioral phenotype observed in KBG syndrome caused by ANKRD11 mutations. Am. J. Med. Genet. B 162b, 17-23 (2013).
- I. Parenti et al., Broadening of cohesinopathies: Exome sequencing identifies mutations in ANKRD11 in two patients with Cornelia de Lange-overlapping phenotype. Clin. Genet. 89, 74-81
- L. Avagliano et al., Chromatinopathies: A focus on Cornelia de Lange syndrome. Clin. Genet. 97,
- 11. F. Cucco et al., Pathogenic variants in and in patients with phenotypes overlapping Cornelia de Lange syndrome. Am. J. Med. Genet. A 182, 1690-1696 (2020).
- 12. I. Parenti, F. J. Kaiser, Cornelia de Lange syndrome as paradigm of chromatinopathies. Front. Neurosci. 15, 774950 (2021).
- 13. I. D. Krantz et al., Cornelia de Lange syndrome is caused by mutations in NIPBL, the human homolog of Drosophila melanogaster Nipped-B. Nat. Genet. 36, 631-635 (2004).
- J. Liu, I. D. Krantz, Cornelia de Lange syndrome, cohesin, and beyond. Clin. Genet. 76, 303-314
- 15. G. Olley et al., BRD4 interacts with NIPBL and BRD4 is mutated in a Cornelia de Lange-like syndrome. Nat. Genet. 50, 329-332 (2018).
- 16. A. D. Kline et al., Diagnosis and management of Cornelia de Lange syndrome: First international consensus statement. Nat. Rev. Genet. 19, 649-666 (2018).
- M. Chen, X. Yang, H. Liu, J. Wan, Identification and functional characterization of a bipartite nuclear localization signal in ANKRD11. Biochem. Biophys. Res. Commun. 670, 117-123 (2023).
- 18. A. Zhang, C. W. Li, S. C. Tsai, J. D. Chen, Subcellular localization of ankyrin repeats cofactor-1 regulates its corepressor activity. J. Cell Biochem. 101, 1301-1315 (2007)
- 19. D. Gallagher et al., Ankrd11 is a chromatin regulator involved in autism that is essential for neural development. Dev. Cell 32, 31-42 (2015).

significance accepted at P < 0.05. Power calculations were performed using GraphPad Prism v9.0.

Data, Materials, and Software Availability. Atomic coordinates of the ANKRD11\_342-378/STAG2-RAD21 complex are available at the Protein Data Bank (PDB: 9J0A) (65). RNA-seq data are deposited in GEO (GSE273955) (66) and the Genome Sequence Archive (GSA: CRA018141) (67). All other data and methods are included in the manuscript and *SI Appendix*.

**ACKNOWLEDGMENTS.** We thank the BL18U1 beamline at the National Facility for Protein Science Shanghai for X-ray beam time. This work was supported by grants from Key-Area Research and Development Program of Guangdong Province (2023B0303010001), the National Natural Science Foundation of China (82188101), the Ministry of Science and Technology of China (2019YFA0508402), Shenzhen Bay Laboratory (S201101002), Shenzhen Talent Program (KQTD20210811090115021), Shenzhen Science and Technology Basic Research Program (JCYJ20220818100215033), Shenzhen Science and Technology Program (ZDSYS20220402111000001), Guangdong Innovative and Entrepreneurial Research Team Program (2021ZT09Y104), and Shenzhen Medical Research Fund (B2302039) to M.Z., National Natural Science Foundation of China (Grants: 31721002, 81920208014, and 31930051 to Youming Lu and 32200795 to H. Li), and Natural Science Foundation of Hubei Province (2022CFB608) to H. Li.

Author affiliations: aShenzhen Key Laboratory of Biomolecular Assembling and Regulation, Department of Neuroscience, School of Life Sciences, Southern University of Science and Technology, Shenzhen 518055, China; <sup>b</sup>Greater Bay Biomedical Innocenter, Shenzhen Bay Laboratory, Shenzhen 518036, China; Department of Pathophysiology, School of Basic Medicine and Tongji Medical College, Huazhong University of Science and Technology, Wuhan 430030, China; <sup>d</sup>The Institute for Brain Research, Collaborative Innovation Center for Brain Science, Huazhong University of Science and Technology, Wuhan 430030, China; <sup>e</sup>Department of Laboratory Medicine, State Key Laboratory of Vaccines for Infectious Diseases, School of Public Health, Xiamen University, Xiamen, Fujian 361102, China; <sup>f</sup>State Key Laboratory of Respiratory Disease, Guangzhou Institutes of Biomedicine and Health, Chinese Academy of Sciences, Guangzhou 510530, China; <sup>g</sup>Guangzhou National Laboratory, Guangzhou 510005, China; and <sup>h</sup>University of Chinese Academy of Sciences, Beijing 100049, China

- 20. K. Walz et al., Characterization of ANKRD11 mutations in humans and mice related to KBG syndrome. Hum. Genet. 134, 181-190 (2015).
- D. M. Roth et al., The chromatin regulator Ankrd11 controls palate and cranial bone development. Front. Cell Dev. Biol. 9, 645386 (2021).
- 22. Y. Kibalnyk et al., The chromatin regulator Ankrd11 controls cardiac neural crest cell-mediated outflow tract remodeling and heart function. Nat. Commun. 15, 4632 (2024).
- 23. I. Barbaric et al., An ENU-induced mutation in the Ankrd11 gene results in an osteopenia-like phenotype in the mouse mutant Yoda. Physiol. Genomics 32, 311-321 (2008).
- S. Yatskevich, J. Rhodes, K. Nasmyth, Organization of chromosomal DNA by SMC complexes. Annu. Rev. Genet. 53, 445-482 (2019).
- 25. J. E. Phillips-Cremins et al., Architectural protein subclasses shape 3D organization of genomes during lineage commitment. Cell 153, 1281-1295 (2013).
- I. Litwin, E. Pilarczyk, R. Wysocki, The emerging role of cohesin in the DNA damage response. Genes-Basel 9, 581 (2018).
- A. Piazza et al., Cohesin regulates homology search during recombinational DNA repair. Nat. Cell Biol. 23, 1176-1186 (2021).
- J. M. Peters, A. Tedeschi, J. Schmitz, The cohesin complex and its roles in chromosome biology. Gene Dev. 22, 3089-3114 (2008).
- J. H. I. Haarhuis, A. M. O. Elbatsh, B. D. Rowland, Cohesin and its regulation: On the logic of X-shaped chromosomes. Dev. Cell 31, 7-18 (2014).
- I. F. Davidson, J. M. Peters, Genome folding through loop extrusion by SMC complexes. Nat. Rev. Mol. Cell Bio. 22, 445-464 (2021).
- 31. J. R. Dixon et al., Topological domains in mammalian genomes identified by analysis of chromatin interactions. Nature 485, 376-381 (2012).
- W. Schwarzer et al., Two independent modes of chromatin organization revealed by cohesin removal. Nature 551, 51-56 (2017).
- S. S. P. Rao et al., Cohesin loss eliminates all loop domains. Cell 171, 305-320.e24 (2017).
- Y. Kim, Z. B. Shi, H. S. Zhang, I. J. Finkelstein, H. T. Yu, Human cohesin compacts DNA by loop extrusion. Science 366, 1345-1349 (2019).
- I. F. Davidson et al., DNA loop extrusion by human cohesin. Science 366, 1338-1345 (2019).
- B. Yuan et al., Global transcriptional disturbances underlie Cornelia de Lange syndrome and related phenotypes. J. Clin. Invest. 125, 636-651 (2015).
- J. Liu et al., Transcriptional dysregulation in NIPBL and cohesin mutant human cells. PLoS Biol. 7, e1000119 (2009).
- R. Linares-Saldana et al., BRD4 orchestrates genome folding to promote neural crest differentiation. Nat. Genet. 53, 1480-1492 (2021).
- N. Luna-Pelaez et al., The Cornelia de Lange syndrome-associated factor NIPBL interacts with BRD4 ET domain for transcription control of a common set of genes. Cell Death Dis. 10, 548 (2019).

- J. S. Kim et al., Systematic proteomics of endogenous human cohesin reveals an interaction with diverse splicing factors and RNA-binding proteins required for mitotic progression. J. Biol. Chem. 294, 8760–8772 (2019).
- 41. Y. Li *et al.*, The structural basis for cohesin-CTCF-anchored loops. *Nature* **578**, 472-476
- A. Garcia-Nieto et al., Structural basis of centromeric cohesion protection. Nat. Struct. Mol. Biol. 30, 853–859 (2023).
- B. J. H. Dequeker et al., MCM complexes are barriers that restrict cohesin-mediated loop extrusion. Nature 606, 197–203 (2022).
- A. L. Nguyen, E. Smith, I. M. Cheeseman, Co-essentiality analysis identifies PRR12 as a regulator of cohesin and genome integrity. bioXriv [Preprint] (2024). https://www.biorxiv.org/ content/10.1101/2024.03.29.587394v1 (Accessed 1 April 2024).
- J. J. M. van Schie et al., CRISPR screens in sister chromatid cohesion defective cells reveal PAXIP1-PAGR1 as regulator of chromatin association of cohesin. Nucleic Acids Res. 51, 9594-9609 (2023)
- I. Mayayo-Peralta et al., PAXIP1 and STAG2 converge to maintain 3D genome architecture and facilitate promoter/enhancer contacts to enable stress hormone-dependent transcription. Nucleic Acids Res. 51, 9576-9593 (2023).
- M. S. Leduc et al., De novo apparent loss-of-function mutations in three patients with intellectual disability and iris abnormalities. Hum. Genet. 137, 257-264 (2018).
- F. Chowdhury et al., Haploinsufficiency of PRR12 causes a spectrum of neurodevelopmental, eye, and multisystem abnormalities. Genet. Med. 23, 1234–1245 (2021).
- H. Daum et al., Bi-allelic PAGR1 variants are associated with microcephaly and a severe neurodevelopmental disorder: Genetic evidence from two families. Am. J. Med. Genet. A 188, 336–349 (2022).
- J. Li et al., An alternative CTCF isoform antagonizes canonical CTCF occupancy and changes chromatin architecture to promote apoptosis. Nat. Commun. 10, 1535 (2019).
- T. S. Hsieh et al., Enhancer-promoter interactions and transcription are largely maintained upon acute loss of CTCF, cohesin, WAPL or YY1. Nat. Genet. 54, 1919-1932 (2022).
- H. Zimmerman, Z. Y. Yin, F. Zou, E. T. Everett, Interfrontal bone among inbred strains of mice and QTL mapping. Front. Genet. 10, 291 (2019).
- F. Demaria et al., Obsessive compulsive "paper handling": A potential distinctive behavior in children and adolescents with KBG syndrome. J. Clin. Med. 11, 4687 (2022).

- P. Alfieri et al., Obsessive compulsive symptoms and psychopathological profile in children and adolescents with KBG syndrome. Brain Sci. 9, 313 (2019).
- M. Merkenschlager, D. T. Odom, CTCF and cohesin: Linking gene regulatory elements with their targets. Cell 152, 1285–1297 (2013).
- C. T. Ong, V. G. Corces, CTCF: An architectural protein bridging genome topology and function. Nat. Rev. Genet. 15, 234–246 (2014).
- N. L. Rittenhouse, J. M. Dowen, Cohesin regulation and roles in chromosome structure and function. Curr. Opin. Genet. Dev. 85, 102159 (2024).
- T. Nakagawa, S. Hattori, T. Hosoi, K. Nakayama, Neurobehavioral characteristics of mice with SETD5 mutations as models of IDD23 and KBG syndromes. Front. Genet. 13, 1022339 (2022).
- I. R. Fernandes et al., Genetic variations on SETD5 underlying autistic conditions. Dev. Neurobiol. 78, 500-518 (2018).
- M. Crippa et al., SETD5 gene haploinsufficiency in three patients with suspected KBG syndrome. Front. Neurol. 11, 631 (2020).
- G. Pascolini, M. Gnazzo, A. Novelli, P. Grammatico, Clinical refinement of the SETD5-associated phenotype in a child displaying novel features and KBG syndrome-like appearance. Am. J. Med. Genet. A 188, 1623–1625 (2022).
- E. Deliu et al., Haploinsufficiency of the intellectual disability gene SETD5 disturbs developmental gene expression and cognition. Nat. Neurosci. 21, 1717–1727 (2018).
- A. B. Osipovich, R. Gangula, P. G. Vianna, M. A. Magnuson, is essential for mammalian development and the co-transcriptional regulation of histone acetylation. *Development* 143, 4595–4607 (2016).
- H. G. Valverde de Morales, H. L. Wang, K. Garber, V. Corces, H. Li, "CTCF-related disorder" in GeneReviews 

  [Internet], M. P. Adam et al., Eds. (University of Washington, Seattle, WA, 1993-2025). https://www.ncbi.nlm.nih.gov/sites/books/NBK603087/.
- H. Liu, Q. Cai, M. Zhang, Data from "Complex structure of ANKRD11/STAG2/RAD21." Protein Data Bank. https://www.rcsb.org/structure/9J0A. Deposited 2 August 2024.
- H. Liu et al., Data from "ANKRD11 binding to cohesin suggests a connection between KBG syndrome and Cornelia de Lange syndrome." GEO. https://submit.ncbi.nlm.nih.gov/geo/ submission/update/?acc=GSE273955. Deposited 4 August 2024.
- H. Liu et al., Data from "ANKRD11 binding to cohesin suggests a connection between KBG syndrome and Cornelia de Lange syndrome." GSA. https://ngdc.cncb.ac.cn/gsa/s/h375PZJr. Deposited 1 August 2024.